Supplementary data of experiment

A synergistic co-passivation strategy for high performance perovskite solar cells with large open circuit voltage

Yan Feng,[a] Rong Liu,[a] Fumin Li,[a]* Mengqi Jin,[a] Qing Du,[a] Yanjing Rong,[a] Hangyu Hu,[a] Mengxin Wang,[a] Yu Li,[a] Zhitao Shen,[a] Ying Liu,[a] Huilin Li,[a]* Chong Chen[a]*

[a] Henan Key Laboratory of Photovoltaic Materials, Henan University, Kaifeng 475004, P. R. China

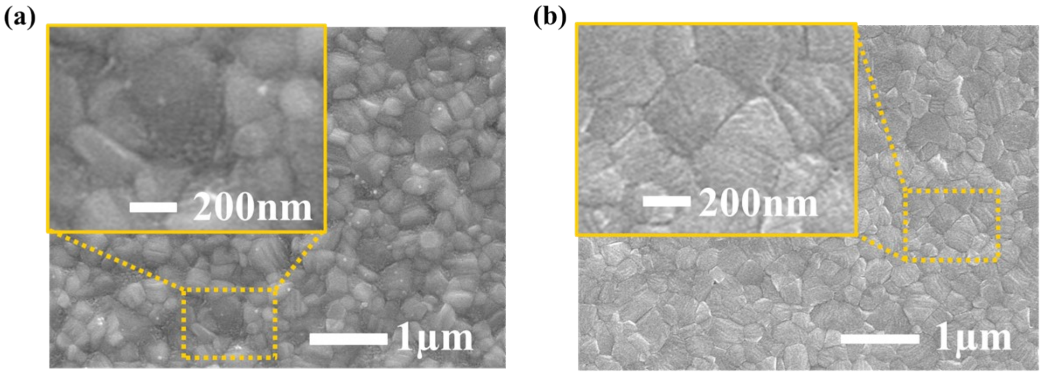

Figure. S1. Top-view of scanning electron microscopy (SEM) image of (a) ITO/SnO_2-KCl/KF/CFM/M-QDs film, and (b) ITO/SnO_2-KCl/KF/CFM/OAI film.

Note: CFM, M-QDs and OAI are the abbreviations of $Cs_{0.05}(FA_{0.85}MA_{0.15})_{0.95}Pb(I_{0.85}Br_{0.15})_3$, $MAPbBr_3$ quantum-dots, and n-octylammonium iodide, respectively.

E-mail: lifm@henu.edu.cn (F. Li), leehl@henu.edu.cn (H. Li) and chongchen@henu.edu.cn (C. Chen).

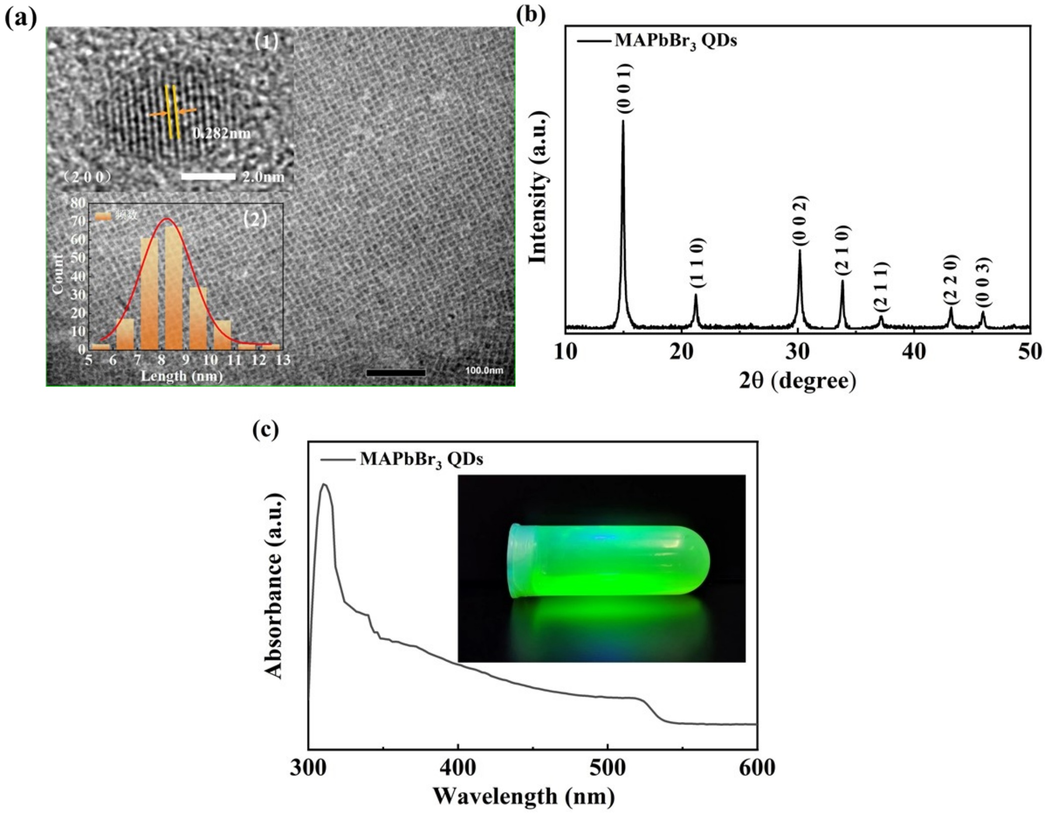

Figure S2. Characterization of morphological and optical properties for M-QDs (a) TEM, the insets show the lattice stripe image and statistical chart of quantum dot size, (b) XRD patten, (c) UV-vis absorption spectra, the inset shows the image of M-QDs solution under UV lamp.

Note for Figure S2: Transmission electron microscopy (TEM) were performed to determine the size and mass of the prepared M-QDs (Fig. S2a). The M-QDs have a uniform grain size which statistical data (the inset 2 in Fig. S2a) yielded an average of 8.6 nm, demonstrating their quantum nature and neat alignment. The lattice stripes (the inset 1 in Fig. S2a) show a lattice spacing of 2.82 Å, which is consistent with the (0 0 2) crystal plane, according to the X-ray diffraction (XRD) result (in Fig. S2b). Fig. S2c shows the ultraviolet-visible (UV-vis) absorption spectra of the M-QDs film, in which the absorption edge is about 540 nm, corresponding to the phenomenon of emitting green fluorescence of QDs (the inset in Fig. S2c).

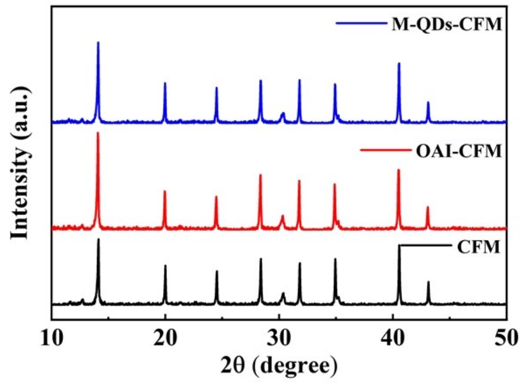

Figure S3. XRD pattens of OAI-CFM, M-QDs-CFM and control CFM films.

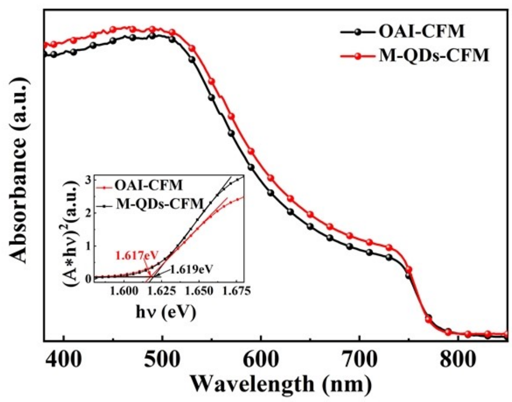

Figure S4. UV-vis absorption spectra of OAI-CFM and M-QDs-CFM. The inset shows their band gap.

Table S1. Fitted parameters of TRPL spectrta of control CFM and TSTP CFM films quartz substrates. The τ_{avg} is calculated from the equation of $\tau_{avg}=(A_1*\tau_1^2+A_2*\tau_2^2)/\ (A_1*\tau_1+A_2*\tau_2)$.

	A_1(%)	τ_1 (μs)	A_2(%)	τ_2 (μs)	τ_{avg} (μs)
Control CFM	10.4	0.75	89.5	2.16	2.11
TSTP-CFM	76.04	0.11	23.96	6.04	5.72

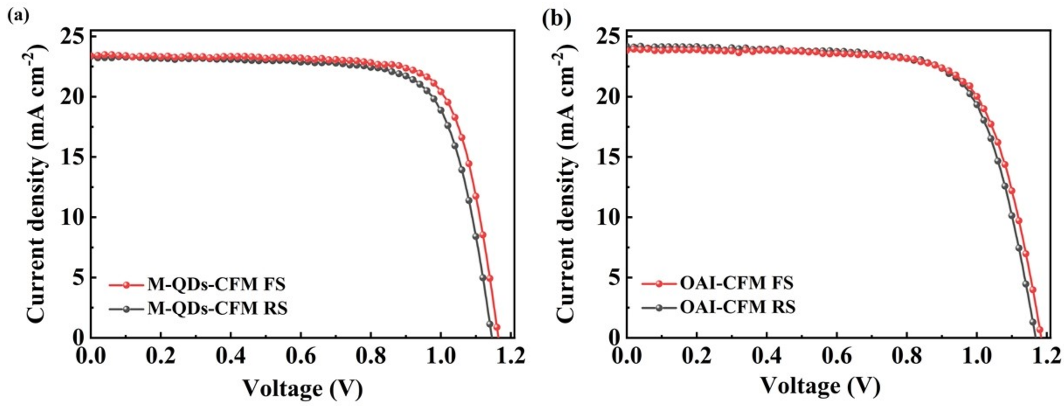

Figure S5. The current density-voltage (*J-V*) characteristic of (a) M-QDs-CFM, (b) OAI-CFM devices, including forward scans (FS) and reverse scans (RS).

Table S2. Performance parameters for FS and RS of the control CFM and TSTP-CFM devices. The hysteresis index (HI) is determined using the equation of HI = $(PCE_{FS}-PCE_{RS})/PCE_{FS}$.

	V_{oc} (V)	J_{sc} (mA cm^{-2})	PCE (%)	FF	HI(%)
M-QDs-CFM FS	1.17	23.40	20.81%	0.76	6.3%
M-QDs-CFM RS	1.15	23.24	19.51%	0.73	
OAI-CFM FS	1.18	23.83	20.53%	0.73	0.8%
OAI-CFM RS	1.17	24.17	20.36%	0.72	

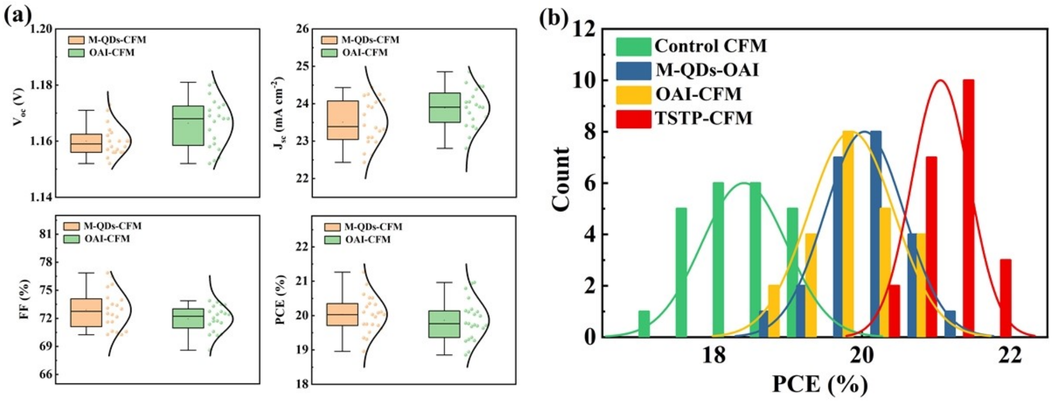

Figure S6. (a) Statistical plot of *J*-*V* parameters based on M-QDs-CFM and OAI-CFM devices, (b) PCE statistical chart of four different structure devices in this work.

Table S3. The electrochemical impedance spectroscopy (EIS) fitting results of Control CFM and TSTP-CFM devices.

	R_s (Ω cm^2)	R_{trans} (Ω cm^2)	R_{rec} (Ω cm^2)	C_{trans} (μF cm^{-2})	C_{rec} (μF cm^{-2})
Control CFM	72	400.7	365.8	0.88	0.73
TSTP-CFM	59.5	282.8	891.9	1.09	0.85

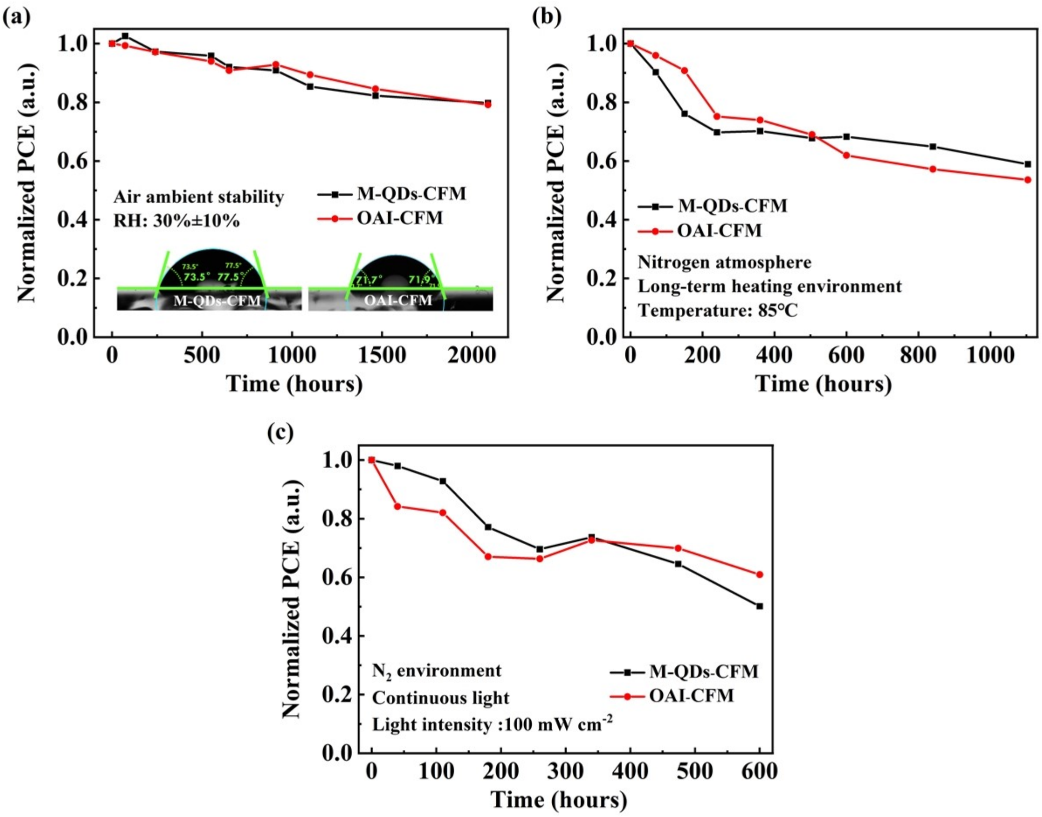

Fig. S7. Long-term stability of un-encapsulated devices based on the OAI-CFM and M-QDs-CFM (a) in air with a relative humidity of ~30%, (b) in an N_2 environment at constant temperature of 85°C, and (c) in an N_2 environment under continuous light soaking at 100 mW cm^{-2}.

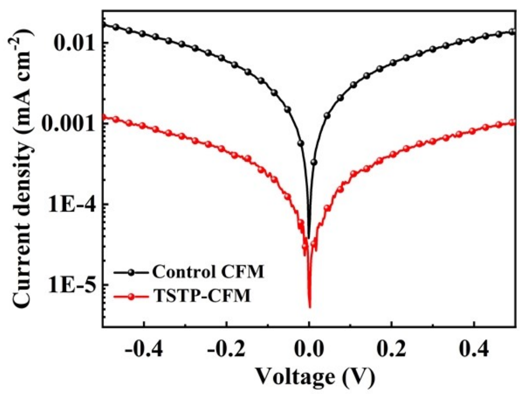

Figure S8. *J-V* characteristics of the control CFM and TSTP-CFM devices scanning from -0.5 V to 0.5 V in the dark.